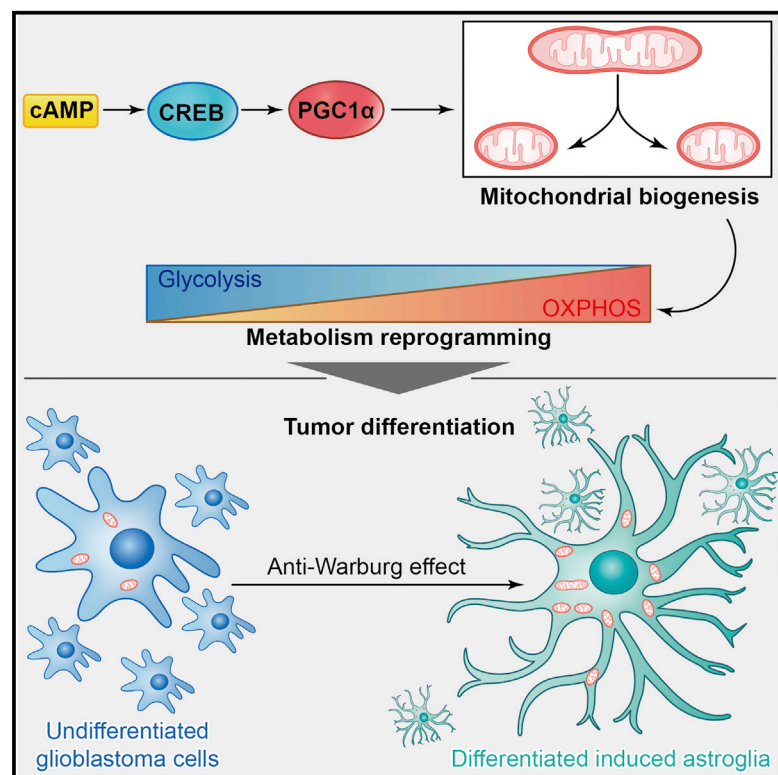


## The Anti-Warburg Effect Elicited by the cAMP-PGC1 $\alpha$ Pathway Drives Differentiation of Glioblastoma Cells into Astrocytes

### Graphical Abstract



### Authors

Fan Xing, Yizhao Luan, Jing Cai, ..., Zhi Xie, Wenbo Zhu, Guangmei Yan

### Correspondence

xiezhi@gmail.com (Z.X.),  
zhuwenbo@mail.sysu.edu.cn (W.Z.),  
ygm@mail.sysu.edu.cn (G.Y.)

### In Brief

Xing et al. show that the metabolic shift from glycolysis to oxidative phosphorylation drives differentiation of GBM cells into astrocytes by cAMP phosphorylation. Mechanistically, the cAMP-CREB-PGC1 $\alpha$  signal mediates mitochondrial biogenesis, which leads to metabolic reprogramming, induced differentiation, and tumor growth inhibition.

### Highlights

- The anti-Warburg effect is elicited by cAMP activation in GBM cells
- Metabolic switch to oxidative phosphorylation drives the differentiation of GBM
- Mitochondrial biogenesis by cAMP activation triggers metabolic reprogramming
- The cAMP-CREB-PGC1 $\alpha$  signal induces mitochondrial biogenesis and metabolic shift

### Accession Numbers

GSE89745  
PXD005334



# The Anti-Warburg Effect Elicited by the cAMP-PGC1 $\alpha$ Pathway Drives Differentiation of Glioblastoma Cells into Astrocytes

Fan Xing,<sup>1,10</sup> Yizhao Luan,<sup>3,4,10</sup> Jing Cai,<sup>1,10</sup> Sihan Wu,<sup>1</sup> Jialuo Mai,<sup>1</sup> Jiayu Gu,<sup>1</sup> Haipeng Zhang,<sup>1</sup> Kai Li,<sup>1</sup> Yuan Lin,<sup>1</sup> Xiao Xiao,<sup>1</sup> Jiankai Liang,<sup>1</sup> Yuan Li,<sup>1</sup> Wenli Chen,<sup>1</sup> Yaqian Tan,<sup>1</sup> Longxiang Sheng,<sup>1</sup> Bingzheng Lu,<sup>1</sup> Wanjun Lu,<sup>1</sup> Mingshi Gao,<sup>1</sup> Pengxin Qiu,<sup>1</sup> Xingwen Su,<sup>1</sup> Wei Yin,<sup>5</sup> Jun Hu,<sup>6</sup> Zhongping Chen,<sup>2,7</sup> Ke Sai,<sup>2,7</sup> Jing Wang,<sup>2,7</sup> Furong Chen,<sup>2,7</sup> Yinsheng Chen,<sup>2,7</sup> Shida Zhu,<sup>8</sup> Dongbing Liu,<sup>8</sup> Shiyuan Cheng,<sup>9</sup> Zhi Xie,<sup>3,\*</sup> Wenbo Zhu,<sup>1,\*</sup> and Guangmei Yan<sup>1,2,11,\*</sup>

<sup>1</sup>Department of Pharmacology, Zhongshan School of Medicine, Sun Yat-sen University, Guangzhou 510080, China

<sup>2</sup>Collaborative Innovation Center for Cancer Medicine, Guangzhou 510060, China

<sup>3</sup>State Key Lab of Ophthalmology, Guangdong Provincial Key Lab of Ophthalmology and Visual Science, Zhongshan Ophthalmic Center, Sun Yat-sen University, Guangzhou 500040, China

<sup>4</sup>School of Life Sciences, Sun Yat-sen University, Guangzhou 510275, China

<sup>5</sup>Department of Biochemistry, Zhongshan School of Medicine, Sun Yat-sen University, Guangzhou 510080, China

<sup>6</sup>Department of Microbiology, Zhongshan School of Medicine, Sun Yat-sen University, Guangzhou 510080, China

<sup>7</sup>Department of Neurosurgery/Neuro-oncology, Sun Yat-sen University Cancer Center, State Key Laboratory of Oncology in South China, Guangzhou 510060, China

<sup>8</sup>BGI-Shenzhen, Shenzhen 518031, China

<sup>9</sup>Department of Neurology and Northwestern Brain Tumor Institute, Center for Genetic Medicine, H. Robert Lurie Comprehensive Cancer Center, Northwestern University Feinberg School of Medicine, Chicago, IL 60611, USA

<sup>10</sup>Co-first author

<sup>11</sup>Lead Contact

\*Correspondence: [xiezhi@gmail.com](mailto:xiezhi@gmail.com) (Z.X.), [zhuwenbo@mail.sysu.edu.cn](mailto:zhuwenbo@mail.sysu.edu.cn) (W.Z.), [ygm@mail.sysu.edu.cn](mailto:ygm@mail.sysu.edu.cn) (G.Y.)

<http://dx.doi.org/10.1016/j.celrep.2016.12.037>

## SUMMARY

Glioblastoma multiforme (GBM) is among the most aggressive of human cancers. Although differentiation therapy has been proposed as a potential approach to treat GBM, the mechanisms of induced differentiation remain poorly defined. Here, we established an induced differentiation model of GBM using cAMP activators that specifically directed GBM differentiation into astroglia. Transcriptomic and proteomic analyses revealed that oxidative phosphorylation and mitochondrial biogenesis are involved in induced differentiation of GBM. Dibutyl cyclic AMP (dbcAMP) reverses the Warburg effect, as evidenced by increased oxygen consumption and reduced lactate production. Mitochondrial biogenesis induced by activation of the CREB-PGC1 $\alpha$  pathway triggers metabolic shift and differentiation. Blocking mitochondrial biogenesis using mdivi1 or by silencing PGC1 $\alpha$  abrogates differentiation; conversely, overexpression of PGC1 $\alpha$  elicits differentiation. In GBM xenograft models and patient-derived GBM samples, cAMP activators also induce tumor growth inhibition and differentiation. Our data show that mitochondrial biogenesis and metabolic switch to oxidative phosphorylation drive the differentiation of tumor cells.

## INTRODUCTION

Glioblastoma multiforme (GBM) has the highest incidence and mortality rate among primary brain cancers and is associated with a dismal prognosis (Cloughesy et al., 2014; Weller et al., 2013). In the past 20 years, the use of a combined strategy consisting of surgery, radiotherapy, and the alkylating agent temozolomide has only slightly increased the median survival of GBM patients from 12.1 to 14.6 months (Stupp et al., 2005). Therapeutic targets and strategies that improve this bleak outlook are therefore urgently required.

Differentiation therapy, which is mechanistically different from most therapies aiming to kill cancer cells, has demonstrated significant clinical benefits in the treatment of hematologic malignancies (Leszczyniecka et al., 2001). Currently, for patients with acute promyelocytic leukemia, clinical complete remission rates exceed 90% after treatment with the differentiation-inducing agents all-trans-retinoic acid (ATRA) and arsenic trioxide (As<sub>2</sub>O<sub>3</sub>), either individually or in combination (Jiao et al., 2013). However, this predominant differentiation-inducing activity has never been achieved in solid tumors. Using GBM as a model system, we sought to identify the central regulator that drives solid tumor cells toward terminal differentiation.

Cyclic AMP (cAMP) and its downstream signals have been intimately involved in regulating cell growth, metabolic pathways, and the cell cycle of the mammalian cell (Stork and Schmitt, 2002). The importance of cAMP signaling in glioma has been highlighted in several studies. Warrington et al. (2010) reported that phosphodiesterase 4A1-mediated cAMP suppression in the brain promotes gliomagenesis following the

loss of neurofibromatosis-1. The clear correlation of low cAMP levels with enhanced brain tumorigenesis, brain tumor grade, and brain tumor growth has naturally prompted efforts to develop cAMP-elevating approaches for brain tumor treatment (Warrington et al., 2015; Yang et al., 2007). Accumulating evidence suggests that the reactivation of cAMP signaling or exposure of glioma cells to cAMP analogs can decrease the proliferation of glioma and inhibit the growth of xenografted brain tumors (Goldhoff et al., 2008; Yang et al., 2007). Moreover, we have shown previously that cAMP signal activators are able to induce differentiation of malignant glioma cells (Li et al., 2007). In this study, cAMP activator-induced differentiation in GBM creates a useful model to find the crucial regulator required for solid tumor differentiation.

The Warburg effect is the metabolism phenotype of cancer cells, which is primarily glycolytic, even when oxygen is abundant (Koppenol et al., 2011). It was long believed to be merely a byproduct of malignant transformation, but it is now being recognized as a driving force in tumorigenesis (Cairns et al., 2011). Here we present that the metabolic shift from glycolysis to oxidative phosphorylation induced by cAMP activators, termed the “anti-Warburg effect,” directs the differentiation of GBM cells to astrocytes. Here we show that restoring the oxidative metabolism through mitochondrial biogenesis provides a differentiation therapy strategy for cancer.

## RESULTS

### cAMP Activators Induce the Differentiation of GBM Cells into Astrocytes

To establish the induced differentiation model in GBM cells, we examined the response of six GBM cell lines to the cAMP analog dibutyryl cyclic AMP (dbcAMP) and identified DBTRG-05MG and U87MG as the most sensitive ones (Figure S1). After exposure to the cAMP analog dbcAMP for 48 hr, both cell lines demonstrated dominant morphology alteration, characterized by small cell bodies and long, fine, tapering processes (Figure 1A). Another two cAMP signal activators, the adenylate cyclase activator forskolin and the non-selective phosphodiesterase inhibitor luteolin, elicited the same morphology changes of both GBM cell lines as dbcAMP-induced ones (Figure 1A).

To further characterize the induced cell phenotype, we quantified mRNAs associated with specific markers of neurons (*TUBB3*, *MAP2*, and *NEUN*), astrocytes (*GFAP* and *S100B*), and oligodendrocytes (*GALC* and *MOG*) as well as stem cell markers (*NES* and *SOX9*) after treatment of dbcAMP. These data showed that both astrocytes markers, *GFAP* and *S100B*, were upregulated in dbcAMP-treated GBM cells, but none of the neuron or oligodendrocyte markers were increased (Figure 1B). In agreement with the increase in glial fibrillary acidic protein (GFAP) mRNA, western blotting and immunofluorescence revealed that GFAP protein levels were elevated in both GBM cell lines (Figures 1C–1E).

Next, we tested whether the differentiated cells had indeed lost their malignancy potential. The fundamental malignant trait of cancer cells is their ability to sustain proliferation. We therefore investigated the effect of dbcAMP on the proliferation of GBM cells. As shown in Figure 1F, the proportion of proliferating

cells stained by 5-ethynyl-2'-deoxyuridine (EdU) dropped from 20.90% to 3.86% in DBTRG-05MG and from 29.86% to 14.69% in U87MG. To determine whether apoptosis and necrosis are triggered by dbcAMP, we next measured caspase-3 activity and lactate dehydrogenase (LDH) release. No significant differences were observed in both indicators (Figures 1G and 1H), suggesting a non-cytotoxic effect of dbcAMP. However, we observed that a fraction of terminal differentiated cells underwent senescence after 72-hr treatment with dbcAMP (Figure S2), indicating that induced differentiation finally forced cancer cells into irreversible cell senescence. Taken together, dbcAMP specifically directed the differentiation of GBM cells into astrocytes, accompanied by a loss of proliferation.

### Transcriptomic and Proteomic Analyses Reveal Boosted Oxidative Phosphorylation in dbcAMP-Treated Cells

We then aimed to figure out the underlying mechanism of induced differentiation of GBM and, thus, assessed the effect of dbcAMP treatment on global gene expression patterns of the most sensitive cell line, DBTRG-05MG, at the transcriptome and proteome levels using RNA sequencing (RNA-seq) experiments and mass spectrometry (MS)/MS experiments separately. dbcAMP treatment time-dependently increased the number of differentially expressed genes from 689 at 6 hr to 2,046 at 48 hr at the mRNA level (Figure 2A). Notably, cell cycle-related genes (the GO:0022402 gene set) were mostly downregulated, whereas glioma-suppressing genes previously derived from The Cancer Genome Atlas Glioblastoma Multiforme (TCGA-GBM) data (Dong et al., 2010) were largely upregulated (Figure 2B).

To determine the effect of transcriptomic and proteomic changes on biological functions and pathways, we performed gene set enrichment analysis (GSEA). From the RNA-seq data, we found significant differences between the induced differentiated cells and their parental GBM cells in multiple metabolism-related pathways, especially ones relating to mitochondrial dysfunction, oxidative phosphorylation, and ubiquinone biosynthesis, over time (Figure 2C). Meanwhile, the top 20 proteomic-enriched pathways were also related to mitochondrial dysfunction, including the tricarboxylic acid (TCA) cycle, oxidative phosphorylation, and other metabolism-related pathways, in accordance with the transcriptomic analysis (Figure 2D). The heatmap of gene expression relating to oxidative phosphorylation indicates that large-scale upregulation started at 12 hr and was maintained until 48 hr (Figure 2E). Taken together, these results indicate that progressive and large-scale changes in gene expression clustered in metabolism-related pathways following cAMP signal activation, suggesting that dbcAMP-induced GBM cell differentiation is associated with a switch of metabolic state.

### The Anti-Warburg Effect Is Elicited in GBM Cells following Exposure to dbcAMP

To functionally validate the degree to which metabolism is switched in differentiated cells from GBM cells, we measured the oxygen consumption rate (OCR) and extracellular acidification rate (ECAR) following treatment with dbcAMP for 12, 24, or 48 hr. In both GBM cell lines, treatment with dbcAMP markedly elevated OCR values and lowered ECAR values (Figures

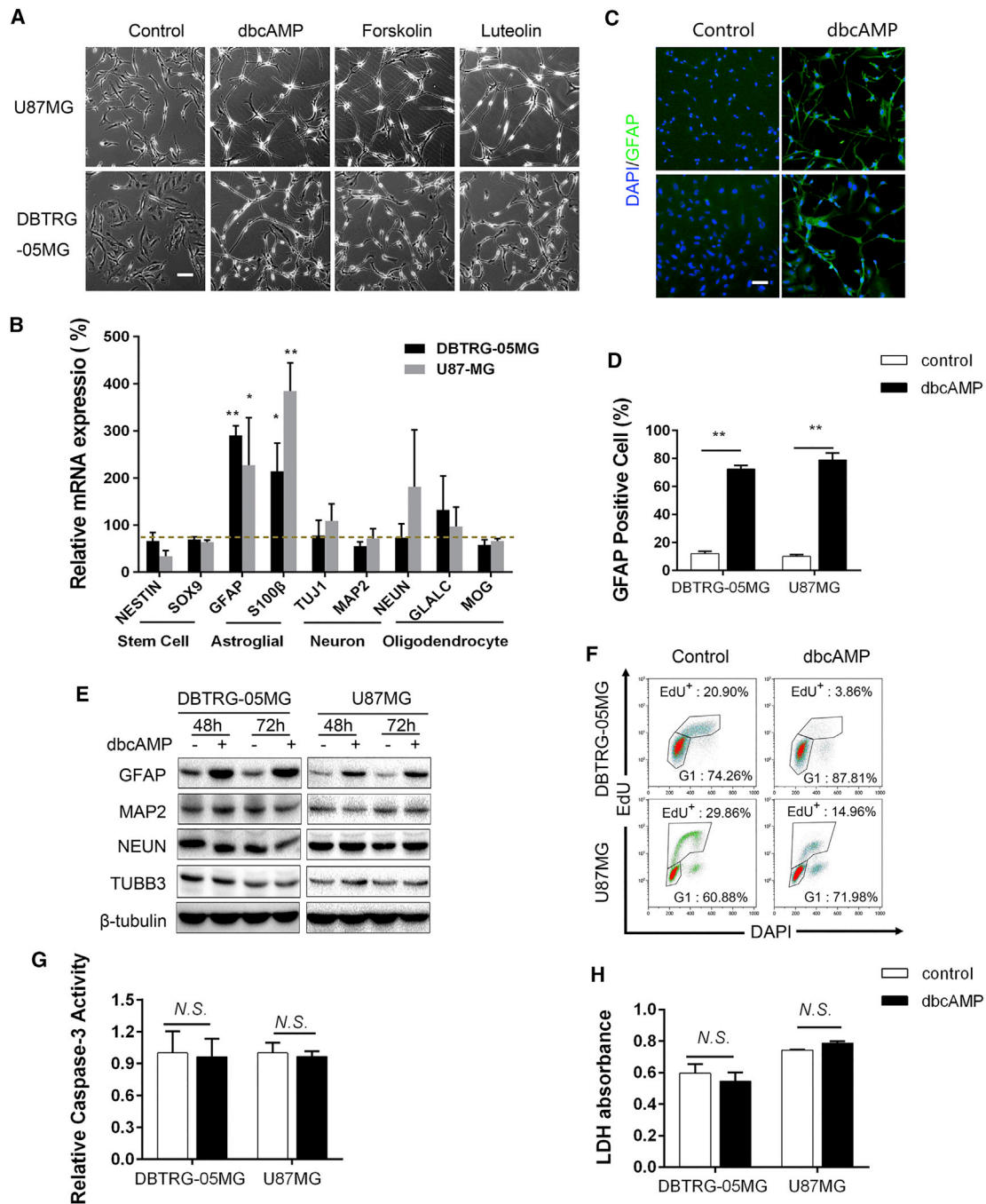


**Figure 1. cAMP Activators Induce Differentiation of GBM Cells without Affecting Cell Death**

(A) The effect of cAMP activators on morphology alteration in DBTRG-05MG and U87MG. Cells were treated with dbcAMP (1 mM), forskolin (50  $\mu$ M), and luteolin (100  $\mu$ M) for 48 hr, and then phase-contrast microscopy images were captured. Scale bar, 100  $\mu$ m.

(B) Relative mRNA levels of markers typical for neurons (*TUBB3*, *MAP2*, and *NEUN*), astrocytes (*GFAP* and *S100B*), oligodendrocytes (*GALC* and *MOG*), and stem cells (*NESTIN* and *SOX9*) by real-time qPCR in two cell lines treated with dbcAMP (1 mM) for 48 hr.

(C and D) Immunofluorescence analysis of GFAP expression (green) in GBM cells treated with 1 mM dbcAMP for 48 hr. DAPI is shown in blue (C). GFAP positive cells were quantified (D). Scale bar, 100  $\mu$ m.

(E) Western blot analysis of GFAP and neuron marker GBM cells treated with 1 mM dbcAMP for 48 and 72 hr. Tubulin was used as a loading control.

(F) The percentage of proliferating EdU-positive cells was determined by flow cytometry. Both cells were treated with 1 mM dbcAMP for 48 hr.

(G and H) Glioma cells were treated with 1 mM dbcAMP for 48 hr, and then cell apoptosis was evaluated by a caspase-3 activity assay (G), and leakage of LDH from GBM cells into the medium was assessed (H).

Mean  $\pm$  SD is shown (n = 3/group). N.S., not significant; \*p < 0.05; \*\*p < 0.01; different from the control group.

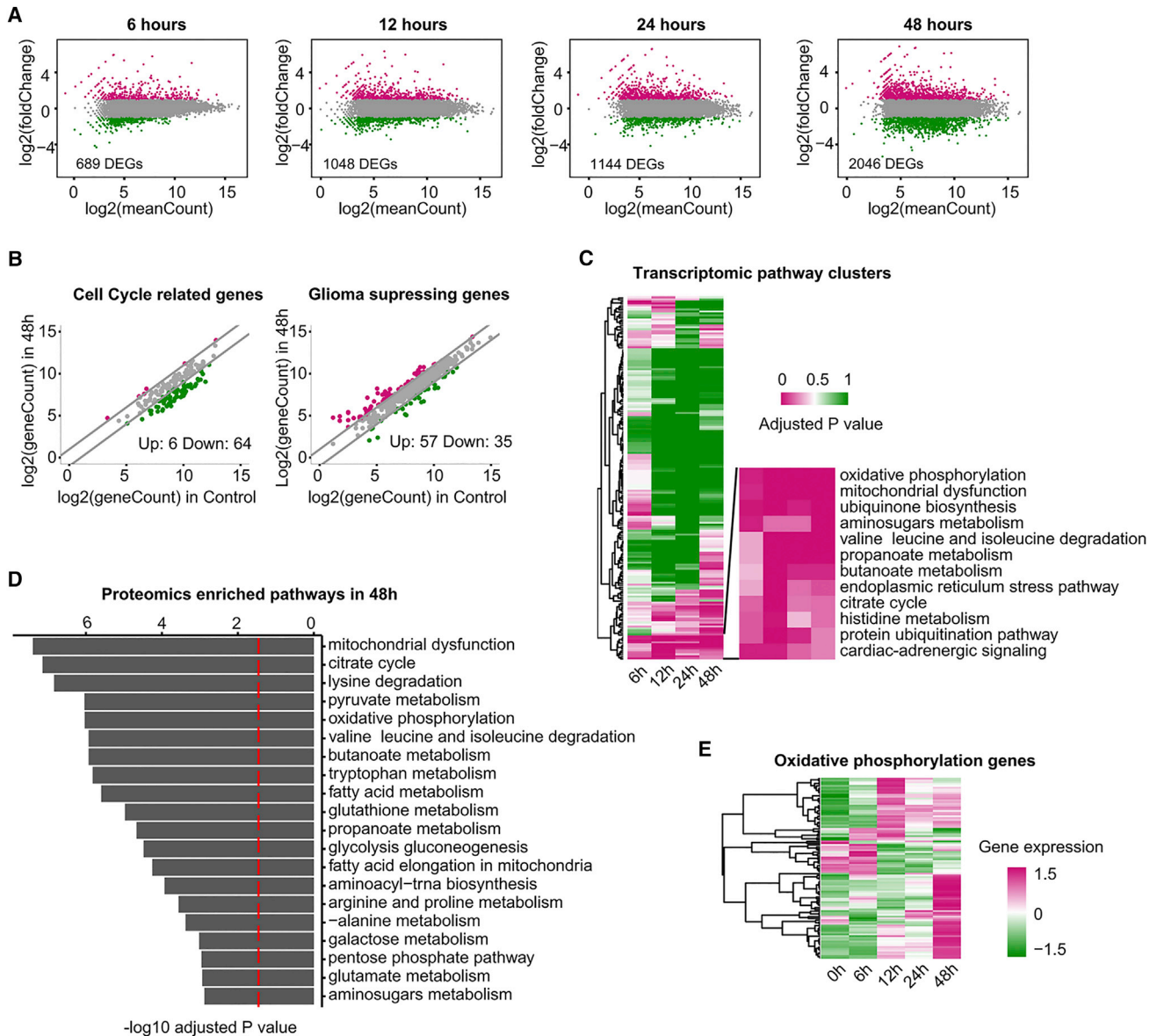


**Figure 2. Transcriptome and Proteomics Profiles Reveal Enhanced Oxidative Metabolism in dbcAMP-Treated Cells**

(A) Log ratio-average (M-A) plots showing changes in gene expression at 6, 12, 24, and 48 hr. The numbers indicate the number of changed genes with fold changes > 2 (red) or < 0.5 (green). Fold change was calculated by dividing the gene expression at the specific time point by that of the control.

(B) Expression changes in cell cycle-related genes (left) and glioma-suppressing genes (right). The gene expression comparison between 0 hr and 48 hr was plotted. Log<sub>2</sub>-normalized gene counts at 0 and 48 hr were used. The upper and lower lines along the diagonal indicate a 2-fold increase or decrease. Upregulated genes are shown in red, and downregulated genes are shown in green.

(C) A gene set enrichment analysis of transcriptome data was performed by comparing four different time points (6, 12, 24, and 48 h) with the control. Metabolic pathways and mitochondrion-related terms were enriched. Adjusted p values were used to plot the heatmap. Hierarchical clustering analysis was performed. Left: the clustering of significance of all ingenuity pathways. Most sensitive pathways are highlighted at the right.

(D) Gene set enrichment analysis of proteomics data performed by comparing the 48-hr time point with the control. Adjusted p values are shown in the bar chart. Red trace lines indicate adjusted p = 0.05.

(E) Heatmap of the expression level of oxidative phosphorylation genes. Z scores were used. High expression is shown in red, and low expression is shown in green.

3A–3D). To test the degree of metabolic shift, we further measured the energy phenotype of cells, which certified that GBM cells processed the metabolic shift from glycolysis to oxidative phosphorylation (Figure S2).

In accordance with the increase in OCR and the decrease in ECAR, the formation of ATP produced by oxidative phosphorylation was elevated (Figure 3E), whereas the level of lactate produced by the glycolytic pathway was reduced (Figure 3F). For a

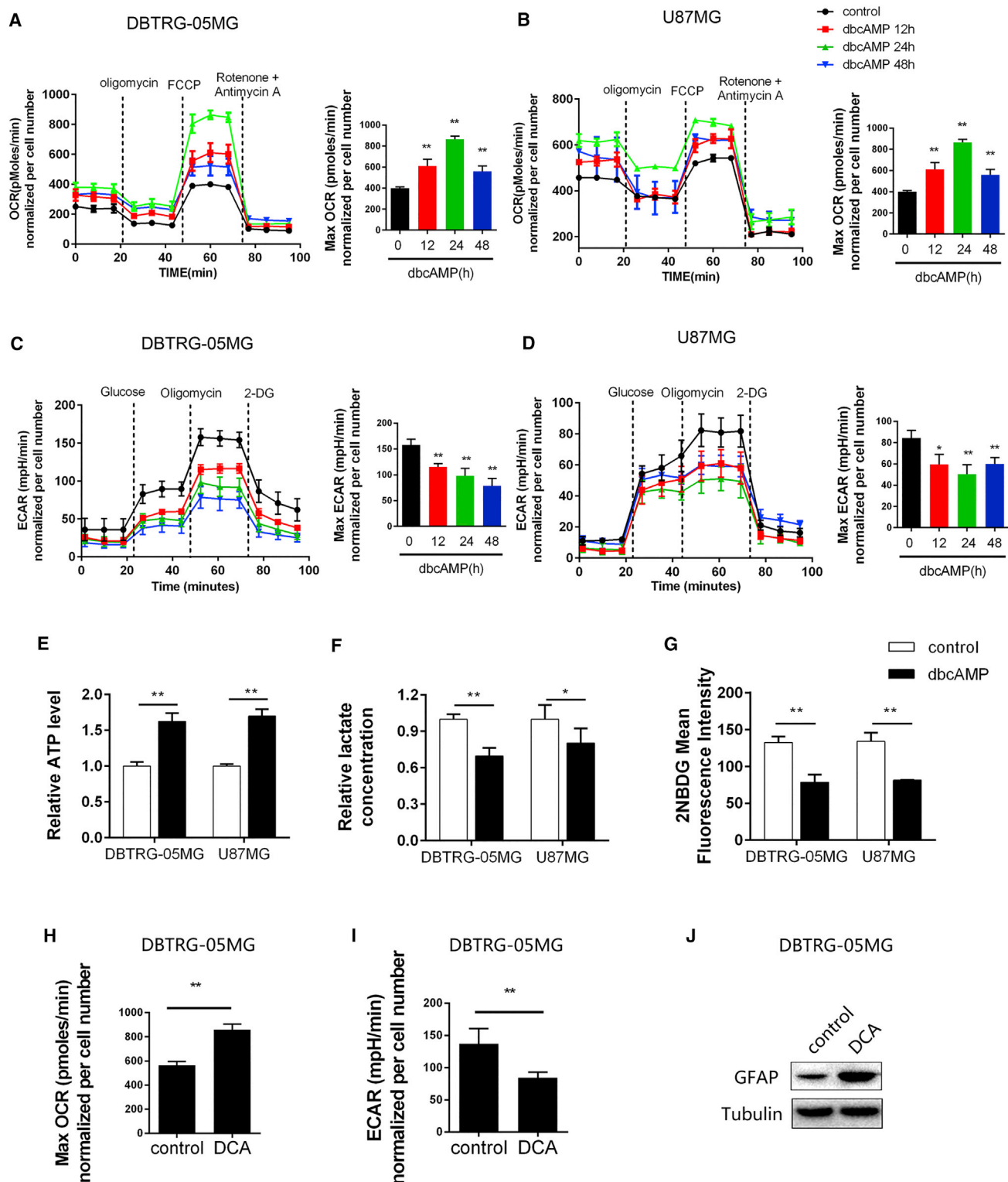


**Figure 3. DbcAMP Treatment Reverses the Warburg Effect**

(A–D) Time-dependent effect of dbcAMP treatment on the OCR and ECAR. Cells were treated with 1 mM dbcAMP for the indicated time, and then the OCR of (A and B) and the ECAR (C and D) were monitored by using the Seahorse Bioscience extracellular flux analyzer in real time. Dotted lines indicate incubation of cells with the indicated compounds.

(E–G) ATP production (E), lactate production (F), and glucose uptake (G) were determined after treatment with 1 mM dbcAMP for 24 hr.

(legend continued on next page)

full characterization of metabolic reprogramming, we included an analysis of glucose uptake. We found that the uptake of a fluorescent glucose derivative, 2-[N-(7-nitrobenz-2-oxa-1,3-diazol-4-yl) amino]-2-deoxy-D-glucose (2-NBDG), was decreased after dbcAMP treatment (Figure 3G). Furthermore, we explored whether other drugs that switch metabolism to oxidative phosphorylation have a similar role in promoting the differentiation of GBM cells. We forced tumor cells to preferentially use oxidative metabolism with dichloroacetate (DCA), which inhibits mitochondrial pyruvate dehydrogenase kinase (Bonnet et al., 2007). We found that DCA treatment similarly induced the metabolic shift (Figures 3H and 3I) and promoted tumor cell differentiation (Figure 3J). Our data suggest that oxidative metabolism is a driver of differentiation but not an accompanied phenomenon during differentiation in GBM cells.

### Mitochondrial Biogenesis Mediates the Metabolic Shift and Leads to GBM Cell Differentiation

Based on the upregulation of mitochondrial component genes observed in the transcriptomic and proteomic analysis, we hypothesized that mitochondrial biogenesis contributes to metabolic reprogramming and GBM cell differentiation. Thus, we first assessed the number and function of mitochondria. Transmission electron microscopy showed that treatment with dbcAMP significantly increased the number of mitochondria in GBM cells (Figures 4A and 4B). Accordingly, dbcAMP treatment increased the fluorescence intensity of MitoTracker Green, a measure of mitochondrial mass (Figure 4C). The mtDNA levels were also elevated in dbcAMP-treated cells (Figure 4D).

To investigate whether the number of mitochondria was increased to compensate for impaired function, we measured the mitochondrial membrane potential using tetramethylrhodamine methyl ester (TMRE). We found a higher TMRE fluorescence intensity in dbcAMP-treated cells (Figure 4E), suggesting that dbcAMP treatment did not impair mitochondrial function.

Mitochondria are remarkably dynamic organelles that divide and fuse (Knott et al., 2008). Mitochondrial fission is required to ensure mitochondrial biogenesis and to respond to changes in energy demands (Jahani-Asl and Slack, 2007; Knott et al., 2008). To further clarify the role of increased mitochondria and their function in the induction of metabolic reprogramming and differentiation of GBM cells, we aimed to abolish the mitochondrial mass induced by dbcAMP by impairing the mitochondrial fission process. When phosphorylated at Ser616, GTPase dynamin-related-protein 1 (Drp1) stimulates mitochondrial fission during mitosis (Knott et al., 2008). We found that dbcAMP increased the phosphorylation of Drp1 at Ser616, indicating that mitochondrial fission was promoted in dbcAMP-treated cells (Figure 4F). Mitochondrial division inhibitor 1 (mdivi-1), working through the selective inhibition of Drp1 (Cassidy-Stone et al., 2008), abolished the induction of oxidative respiration (Figure 4G) and mitochondria (Figure 4H) by dbcAMP. Furthermore, mdivi-1 blocked the stimulated expression of GFAP to varying

extents in DBTRG-05MG and U87MG cells (Figure 4I). Taken together, mitochondrial biogenesis drives the metabolic switch and induces differentiation in GBM cells.

### CREB-PGC1 $\alpha$ Signaling Mediates Mitochondrial Biogenesis in dbcAMP-Treated GBM Cells

The abundance and functional properties of mitochondria are finely tuned to meet the cell's specific energetic, metabolic, and signaling demands (Hock and Kralli, 2009). This tuning is largely achieved by a highly interconnected network of transcription factors (TFs), which regulates a broad set of nuclear genes that encode mitochondrial proteins (Hock and Kralli, 2009). Therefore, we next assessed the ability of the cAMP signal to stimulate these TFs; i.e., NRF1, GA-binding protein (GABP), peroxisome proliferator-activated receptor (PPAR), estrogen-related receptor (ERR), YY-1, and c-MYC (Hock and Kralli, 2009). Dual-Luciferase reporter assays revealed that the transcriptional activities of all tested mitochondrial regulatory TFs were upregulated in dbcAMP-treated U87MG cells (Figure 5A). Based on these data, we postulated that a common regulator of these TFs may be induced, resulting in general transcriptional activation.

The PPAR $\gamma$  coactivator (PGC) family, consisting of PGC1 $\alpha$ , PGC1 $\beta$ , and PGC-1-related coactivator (PRC), is considered the common co-activator of the TFs mentioned above in mitochondrial biogenesis (Hock and Kralli, 2009). In both GBM cell lines we tested, the mRNA level of PGC1 $\alpha$ , but not PGC1 $\beta$  and PRC, was significantly elevated soon after dbcAMP treatment (Figure 5B; Figure S3). Intriguingly, cAMP response element-binding protein (CREB) and AMP-activated protein kinase (AMPK) were respectively responding to cAMP and its metabolite AMP. CREB and AMPK have been reported to regulate the expression of the PGC1 family (Chau et al., 2010; Herzig et al., 2001). These clues drove us to test whether CREB and/or AMPK are responsible for the induction of PGC1 $\alpha$  during GBM cell differentiation. Thus, we determined the protein levels of PGC1 $\alpha$  and the activation states of its upstream molecules CREB and AMPK in both cell lines. PGC1 $\alpha$  was markedly induced, concurrent with an increase in CREB phosphorylation at Ser133 and a decrease in AMPK phosphorylation at Thr172 (Figure 5C). These results demonstrate that a CREB signal, but not an AMPK signal, mediates the stimulation of PGC1 $\alpha$  expression.

To further determine whether PGC1 $\alpha$  is required for the induction of mitochondrial biogenesis and differentiation, we knocked down PGC1 $\alpha$  using specific small interfering RNA (siRNA) fragments. Silencing PGC1 $\alpha$  abrogated the induction of GFAP expression, mtDNA content, and OCR in dbcAMP-treated GBM cells (Figures 5D–5F). We next investigated whether PGC1 $\alpha$  is sufficient to cause tumor cell differentiation. DBTRG-05MG cells were infected with lentiviruses expressing PGC1 $\alpha$  or the empty vector. Overexpression of PGC1 $\alpha$  induced GFAP expression, mtDNA content, and OCR (Figures 5G–5I). Our

(H and I) The effect of DCA treatment on the OCR and ECAR. DBTRG-05MG cells were treated with 10 mM DCA for 24 hr, and then the OCR (H) and the ECAR (I) were determined.

(J) Immunoblot analysis of the differentiation marker GFAP after DCA treatment for 48 hr in DBTRG-05MG cells.

Data are presented as mean  $\pm$  SD ( $n = 3$ /group). \* $p < 0.05$ , \*\* $p < 0.01$ ; different from the control group.

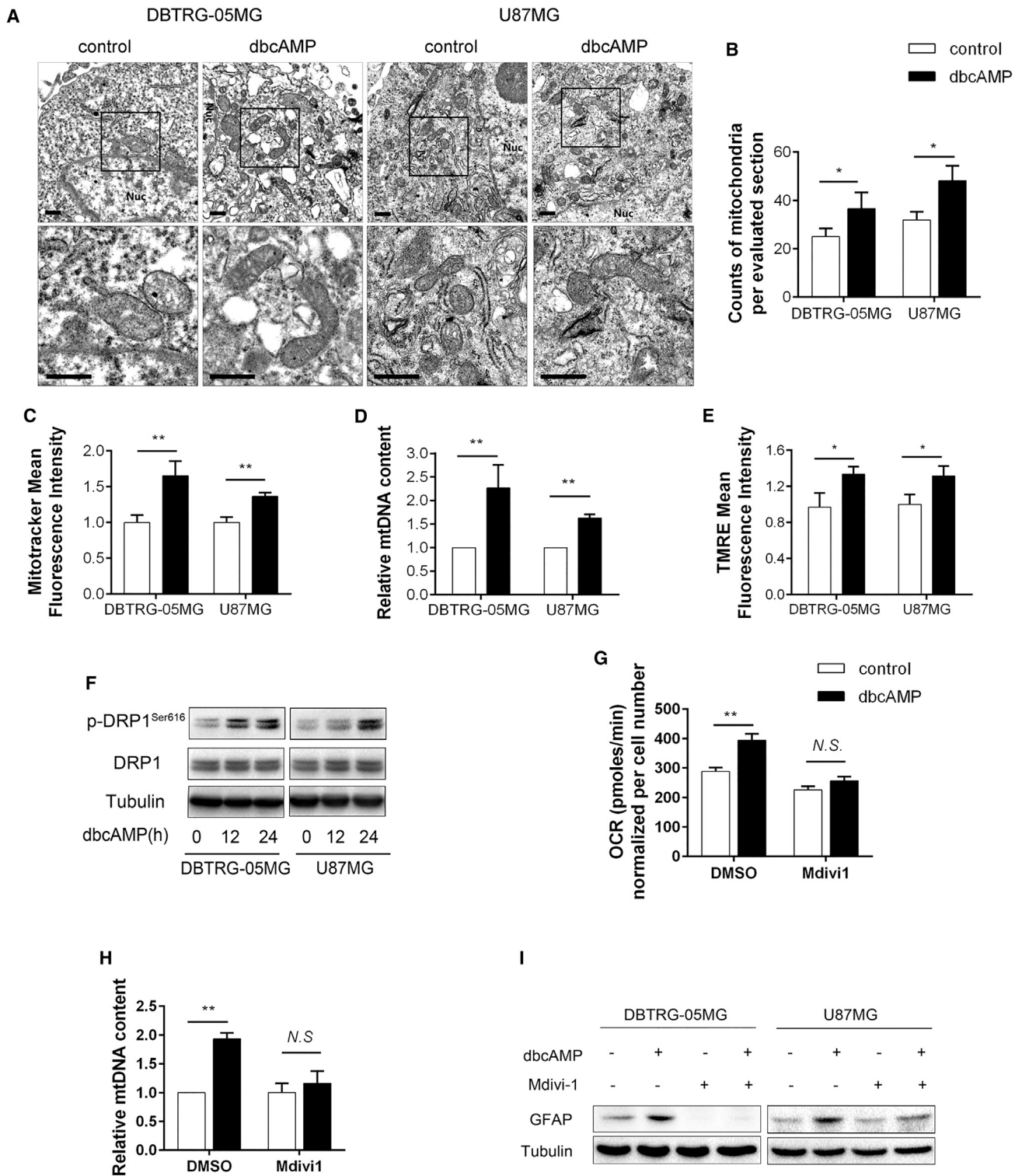


**Figure 4. Mitochondrial Biogenesis Mediates Oxidative Phosphorylation and GFAP Induction by dbcAMP**

(A) Electron micrographs of GBM cells treated with or without dbcAMP. Representative photographs of cells at 22,000 $\times$  (top) or 44,000 $\times$  (bottom) magnification are shown. Red arrowheads indicate representative mitochondria.

(B) Quantification of the number of mitochondria per cell in the imaged section (control, n = 7 cells; dbcAMP, n = 7 cells; two-tailed Student's t test). Data are presented as mean  $\pm$  SD.

(legend continued on next page)

data showed a determinant role of PGC1 $\alpha$  and mitochondrial biogenesis in astroglia differentiation of GBM cells. In addition, silencing of CREB also abolished mitochondrial biogenesis, as evaluated by MitoTracker Green staining (Figure S4A), and inhibited PGC1 $\alpha$  and GFAP expression in dbcAMP-treated GBM cells (Figure S4B). These data suggest that the cAMP-CREB-PGC1 $\alpha$  pathway regulates the mitochondrial biogenesis and differentiation of GBM cells.

### cAMP Activators Induce Tumor Growth Inhibition and Differentiation in GBM Xenograft Models and Patient-Derived GBM Samples

Because cAMP activators induced differentiation and inhibited the growth of GBM cell lines, we next evaluated the anti-tumor and pro-differentiation efficacy of these agents in vivo. In U87MG subcutaneous xenografts in nude mice, we intraperitoneally administrated forskolin (5 mg/kg once per day) and luteolin (5 mg/kg once per day), both of which have a higher liposolubility than dbcAMP. Both forskolin and luteolin potently inhibited tumor growth, as indicated by the tumor growth curves and tumor mass indices (Figure 6A; Figure S5A). No significant difference in body weight was observed in each group (Figure S5B). In addition, treatment with forskolin or luteolin significantly decreased Ki-67 expression (an indicator of cell proliferation) and increased the expression of GFAP (an indicator of cell differentiation) and PGC1 $\alpha$  (an indicator of mitochondrial biogenesis and oxidative phosphorylation) in GBM xenografts (Figures 6B and 6C).

Next, we engineered an orthotopically xenografted model using U87MG cells in nude mice. Mice treated with forskolin or luteolin manifested increased tumor latency relative to mice treated with vehicle (Figure 6E). Kaplan-Meier analysis demonstrated that mice treated with forskolin or luteolin had significantly longer survival times than mice treated with vehicle (Figure 6F).

We further tested whether a similar response was observed in patient-derived GBM samples. After dbcAMP treatment for 48 hr, primary cultured GBM cells also underwent differentiation, as evidenced by the increased level of GFAP (Figures 6F and 6G). The mtDNA content (Figure 6H) and oxidative phosphorylation (Figure 6I) were also increased after dbcAMP treatment. In another orthotopical xenograft model using patient-derived glioma stem cells (GSCs), forskolin treatment (5 mg/kg once per day) also increased the tumor latency and survival of mice (Figures 6J and 6K). Our data revealed that cAMP activators have the capability to repress tumor growth and induce differentiation in vivo and in primary patient-derived GBM samples by restoring oxidative phosphorylation.

## DISCUSSION

Although previous studies have suggested that switching to oxidative phosphorylation plays a central role in the differentiation of normal cells (Folmes et al., 2012), whether restoring oxidative metabolism can direct the differentiation in cancer cells is poorly defined. Here we identified a central role of metabolic reprogramming and mitochondrial biogenesis in regulating the differentiation of cancer cells. The metabolic shift from aerobic glycolysis to oxidative phosphorylation directed GBM cell differentiation into astrocytes, which is termed the anti-Warburg effect. This metabolic reprogramming was triggered by activation of the cAMP-CREB-PGC1 $\alpha$  pathway. Our data strongly support modulation and reprogramming of the metabolic state as a strategy of the differentiation therapy for cancer.

The Warburg effect has been treated as a key metabolic signature in cancer cells (Hsu and Sabatini, 2008; Koppenol et al., 2011). In recent decades, a number of specific inhibitors that target glycolysis enzymes, such as hexokinase 2 (HK2) and lactate dehydrogenase A (LDHA), have demonstrated the ability to selectively kill cancer cells, indicating the potential of targeting the metabolism to inhibit tumors (Galluzzi et al., 2013). In our study, induction of oxidative phosphorylation in response to cAMP activators drives GBM cell differentiation but not cell death. This different outcome of targeting the Warburg effect may be due to the direction of metabolic reprogramming. Actually, consistent with Warburg's initial hypothesis, the suppression of glycolysis and activation of oxidative metabolism are likely separate processes. Thus, instead of inhibiting glycolysis, cAMP activators stimulate mitochondrial biogenesis and oxidative phosphorylation and, eventually, induce cell differentiation. Given that stem cells rely heavily on anaerobic glycolysis, the same as tumor cells, directly targeting glycolysis may increase the risk of causing toxicity to normal stem cells (Ito and Suda, 2014). Therefore, an alternative strategy via inducing oxidative phosphorylation may be safer for cancer therapy.

Cancer metabolic rewiring has been gradually recognized to be involved in malignancy transformation (Losman et al., 2013; Lu et al., 2012). It has been reported that epigenetic metabolites can be oncogenic by altering cell signaling and blocking cellular differentiation, resulting in cancer progression, growth, immune evasion, resistance to treatment, and disease recurrence (Ward and Thompson, 2012). For instance, 2-hydroxyglutarate (2-HG) has recently been shown to drive the malignant transformation of human astrocytes along with the activation of prolylhydroxylases of the EGLN family (Koivunen et al., 2012). Whether disrupting the oncogenic alteration of metabolism could restore the differentiation process is unknown. Here we provide a clear example of induced differentiation by metabolism

(C) MitoTracker Green fluorescence of GBM cells treated with or without dbcAMP (1 mM, 24 hr) was subjected to analysis by flow cytometry.

(D) mtDNA of GBM cells treated with or without dbcAMP (1 mM, 24 hr) was assessed based on the relative level of *ND1* compared with *B3M*.

(E) Mitochondrial membrane potential of GBM cells treated with or without dbcAMP (1 mM, 24 hr) was measured by TMRE staining.

(F) Western blot analyses of Drp1 expression and phosphorylated Drp1 (Ser172) in DBTRG-05MG and U87MG cells treated with dbcAMP (1 mM) for different times.

(G–I) DBTRG-05MG cells were treated with db-cAMP (1 mM), mdivi-1 (25  $\mu$ M), or dbcAMP plus mdivi-1, and then the OCR (G) and mtDNA (H) were measured. The expression of GFAP was detected by western blot analysis following treatment of dbcAMP or mdivi-1 (I).

Data are presented as mean  $\pm$  SD (n = 3/group). \*p < 0.05, \*\*p < 0.01, different from the control group.

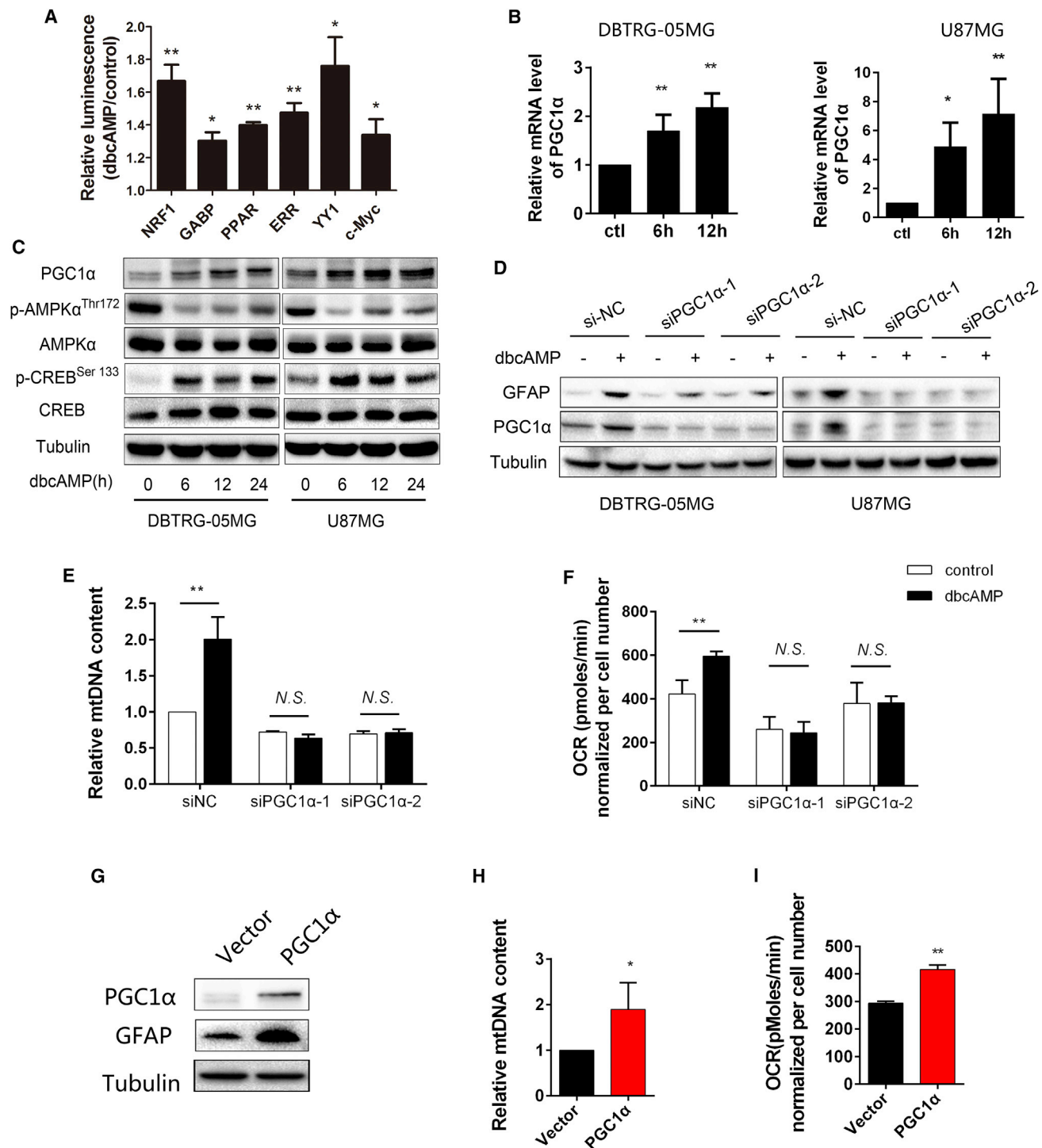


**Figure 5. CREB-PGC1 $\alpha$  Signaling Is Required for Mitochondrial Biogenesis and Induces Differentiation in dbcAMP-Treated GBM Cells**

(A) Dual-Luciferase reporter assays were performed in U87MG cells treated with dbcAMP (1 mM, 24 hr) to measure the transcriptional activity of genes that regulate mitochondrial biogenesis. The data show the relative luminescence of dbcAMP-treated cells compared with control cells.

(B) mRNA levels of PGC1 $\alpha$  were measured by qPCR in DBTRG-05MG and U87MG cells treated with dbcAMP (1 mM) for different times.

(C) Western blot analyses of PGC1 $\alpha$ , phosphorylated AMPK (Thr172), and phosphorylated CREB (Ser133) in DBTRG-05MG and U87MG cells treated with dbcAMP (1 mM) for different times.

(legend continued on next page)

reprogramming, which may be due to the changes in epigenetic metabolites.

PGC1 $\alpha$  has been reported to have a pro- or anti-tumorigenic function in various tumors (LaGory et al., 2015; LeBleu et al., 2014; Sancho et al., 2015; Vazquez et al., 2013), but the reasons for this heterogeneous response remain vague. LeBleu et al. (2014) reported that PGC1 $\alpha$  was highly expressed in circulating tumor cells (CTCs) relative to the primary orthotopic tumor, which promotes CTC invasion and metastasis by facilitating mitochondrial biogenesis and oxidative phosphorylation. In other cancer types, increasing evidence suggests that stimulating PGC1 $\alpha$  expression suppresses tumor growth and enhances sensitivity to cytotoxic therapies by restoring mitochondrial function homeostasis and normalizing oxidative phosphorylation (LaGory et al., 2015; Sancho et al., 2015). In light of these previous findings, the role of PGC1 $\alpha$  in cancer progression may be dual and complex. PGC1 $\alpha$  may interact with different tissue-specific TFs, thus driving distinct molecular pathways in different cancer types. In GBM cells, we identified that PGC1 $\alpha$  plays a central role in inducing differentiation by activating some specific TFs related to mitochondrial biogenesis, including NRF1, GABP, PPAR, and YY1. PGC1 $\alpha$  functions as a tumor suppressor by inducing GBM cells to differentiate into a mature phenotype, and it has strong potential to be developed as a differentiation-inducing target in GBM.

Senescence, as the physiological program of terminal growth arrest, is developed as a potential strategy for cancer treatment (Roninson, 2003). Here, the timeline of induced tumor differentiation and senescence suggest that the final stage of differentiated cells is senescence, as evidenced by the fact that the differentiation marker GFAP is elicited before the senescence marker  $\beta$ -galactosidase (Figure S2). It has been reported that differentiation-inducing anticancer agents such as retinoic acid can cause a senescence-like growth-arrest phenotype in a breast cancer xenotransplant model (Chang et al., 1999), which supports our finding that the final fate of differentiated cells is senescence. In our subcutaneous and intracranial GBM models, besides induction of differentiation, senescence in response to long-term treatment of cAMP activators may also account for the inhibition of cell proliferation and delayed GBM progression.

Among the tested cell lines, we found that a subset of GBM cell lines exhibited less insensitivity to differentiation-inducing agents, which may be due to the presence of inhibitory molecules and/or the lack of essential molecules. The mechanisms underlying the different response to cAMP activators in GBM cells need to be further elucidated. Given the resistance to dbcAMP in some cell lines, further development of alternative oxidative phosphorylation activators should be considered and exploited.

In summary, we mechanistically show that reprogramming the metabolism of GBM cells by stimulating mitochondrial biogenesis promotes GBM cells to transform from a cancerous

phenotype to a mature one. Our data suggest a causal relationship between oxidative metabolism and differentiation in cancer cells. Moreover, our results explore the potential therapeutic relevance of enhancing mitochondrial biogenesis and oxidative metabolism downstream of cAMP signal for treating GBM. We propose that induction of differentiation through metabolism modulation provides a therapy strategy for GBM.

## EXPERIMENTAL PROCEDURES

### Cell Culture and Reagents

All studies involving human glioma samples and animals were approved by the institutional ethics committee of Zhongshan School of Medicine, Sun Yat-sen University.

DBTRG-05MG, U118MG, U87MG, LN-229, T98G, and LN-18 were maintained at 37°C under 5% CO<sub>2</sub> in DMEM supplemented with 10% fetal bovine serum (Gibco) and penicillin/streptomycin. The cell lines were purchased from the American Type Culture Collection.

Primary patient-derived GBM cells and GSCs were provided by Dr. Zhongping Chen (Department of Neurosurgery/Neuro-oncology, Sun Yat-sen University Cancer Center, State Key Laboratory of Oncology in South China, Collaborative Innovation Center for Cancer Medicine). Primary GBM cells were cultured in DMEM/F12 medium supplemented with 10% FBS and penicillin/streptomycin. GSCs were cultured in DMEM/F12 medium supplemented with 2% B27 (Gibco), 20 ng/mL basic fibroblast growth factor (bFGF) (Gibco), and 10 ng/mL epidermal growth factor (EGF) (Gibco).

The following reagents were used in this study: dbcAMP (100 mM, dissolved in double distilled water (ddH<sub>2</sub>O), D0627-1G, Sigma-Aldrich), forskolin (20 mM, dissolved in DMSO, S2449, Selleck Chemicals), luteolin (25  $\mu$ M, dissolved in DMSO, S2320, Selleck Chemicals), and mdvi-1 (25  $\mu$ M, dissolved in DMSO, S7162, Selleck Chemicals).

### qRT-PCR

Total RNA was extracted using TRIzol (Life Technologies) reagent and reverse-transcribed to cDNA using oligo(dT). Specific gene expression was quantified with SuperReal PreMix SYBR Green (TIANGEN) using an Applied Biosystems 7500 fast real-time PCR system (Life Technologies). The following amplification primers (Life Technologies) were used (5' to 3'): GFAP (sense, ACATCGA GATCGCCACCTACA; antisense, GTCTGCACGGGAATGGTGAT), S100B (sense, GGAGACGGCGAATGTGACTT; antisense, GAACTGTGGCAGG CAGTAGTAA), MAP2 (sense, GGGCCTTTTCTTTGAAATCTAGTTT; antisense, CAAA TGTGGCTCTCTGAAGAACA), TUBB3 (sense, GGCCAAGGGTCACTA CACG; antisense, GCAGTCGCAGTTTTCACACTC), NEUN (sense, CCCAT CCCGACTTACGGAG; antisense, GCTGAGCGTATCTGTAGGCT), GALC (sense, GCCAAGCGTTACCATGATTG; antisense, CCACCTGAAGAG TTCGCA), MOG (sense, AGAACGCTACAGGCATGGAG; antisense, CAGGGCTCACCCAGTAGAAAG), NES (sense, CTGCTACCCTTGAGACA CCTG; antisense, GGGCTCTGATCTCTGCATCTAC), SOX9 (sense, CGAAAT CAACGAGAACTGGAC; antisense, ATTTAGCACACTGATCACACG), PGC1 $\alpha$  (sense, AAAGGATGCGCTCTCGTTCA; antisense, CTCAGCC TCTCGTGCTGAT), PGC1 $\beta$  (sense, GAGGTGGACGAGCTCTCACT; antisense, GGGTGTGAGAGCTTG ATGTT), and PRC (sense, CTCCTGGCTACCC CACGTA; antisense, CTCCTGGGAAT GTCAACGC).

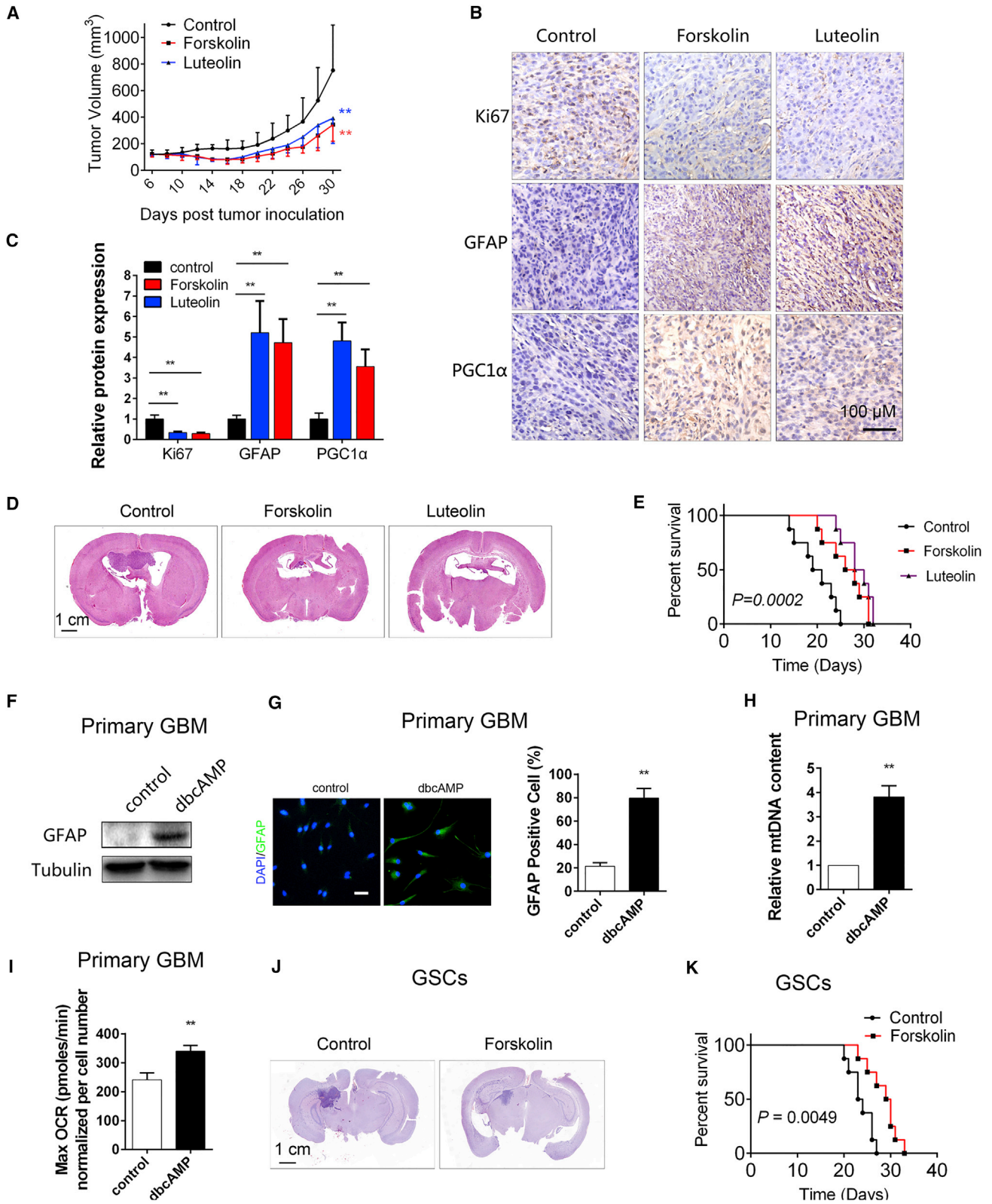
### Western Blotting and Immunohistochemistry

The cells were lysed using M-PER mammalian protein extraction reagent (Thermo Scientific), followed by SDS-PAGE. After being electroblotted onto a polyvinylidene fluoride membrane (Roche), target proteins were detected

(D and E) DBTRG-05MG or U87MG cells were transfected with negative control siRNA (siNC) or siPGC1 $\alpha$  and then treated with 1 mM dbcAMP for 48 hr. Knocking down PGC1 $\alpha$  abrogates the dbcAMP-mediated mtDNA content increase (D) and GFAP upregulation (E).

(G–I) DBTRG-05MG cells were infected with lentiviruses expressing PGC1 $\alpha$  or empty vector. The levels of PGC1 $\alpha$  and GFAP expression were measured (G). Overexpression of PGC1 $\alpha$  induced the mtDNA content (H) and OCR (I) compared with cells transduced with lentiviruses expressing empty vector.

Data are presented as mean  $\pm$  SD (n = 3/group). \*p < 0.05, \*\*p < 0.01, different from the control group.



(legend on next page)

with corresponding antibodies. The following antibodies were used: human GFAP (3670, Cell Signaling Technology), NEUN (ABN51, Millipore), TUBB3 (5568, Cell Signaling Technology), PGC1 $\alpha$  (ab54481, Abcam), CREB (9197, Cell Signaling Technology), Ser133-phosphorylated CREB (9198, Cell Signaling Technology), AMPK $\alpha$  (2532, Cell Signaling Technology), Thr172-phosphorylated AMPK $\alpha$  (2535, Cell Signaling Technology), and tubulin (Ab102, Vazyme).

Immunohistochemistry was performed on 2-mm-thick, formalin-fixed, paraffin-embedded slices. After dewaxing, permeabilizing, and blocking, primary and secondary antibodies were incubated sequentially for detection.

### Transmission Electron Microscopy

DBTRG-05MG and U87MG cells were treated with 1 mM dbcAMP for 24 hr. In brief, the cells were scraped and pelleted at 1,000  $\times$  *g* for 5 min at room temperature. The pellet was then resuspended and washed once with PBS, pelleted again at 1,500  $\times$  *g* for 5 min, and fixed on ice for 4 hr in 0.1 M PBS (pH 7.4) containing 2.5% glutaraldehyde and 2% paraformaldehyde (PFA). The samples were then submitted to the Electron Microscopy Facility at Zhongshan School of Medicine (Sun Yat-sen University) for standard transmission electron microscopy ultrastructural analysis.

### RNAi Experiments

Specific siRNAs targeting PGC1 $\alpha$ , CREB, and protein kinase A (PKA) were purchased from RiboBio. siRNAs were transfected using Lipofectamine RNAiMAX (Life Technologies) with OPTI-MEM (Life Technologies) following the manufacturer's instructions.

### Caspase-3/7 Activity Measurements

The cells were cultured in 96-well plates and treated with 1 mM dbcAMP for 48 hr. Caspase-3/7 activity was assessed using a Caspase-Glo assay system (Promega) according to the manufacturer's protocols. The results were normalized to the cell number determined by a cell counter (Life Technologies).

### Flow Cytometry Analysis

Flow cytometry analysis was performed on a Gallios flow cytometer (Beckman Coulter). For cell proliferation assessment, the cells were incubated with 10  $\mu$ M EdU (Sigma-Aldrich) for 2 hr, and EdU was chemically conjugated to 50  $\mu$ M Auto 488 (Sigma-Aldrich) for 1 hr and incubated with 2.5  $\mu$ g/mL DAPI for another 30 min. For glucose uptake assays in cells, cells were grown under normal conditions, and 100  $\mu$ M 2-NBDG (Invitrogen) was added to the medium for 1 hr.

For mitochondrial mass measurement, MitoTracker Green (Life Technologies) was used to assess the mitochondrial quantity. The cells were incubated for 30 min at 37°C with 50 nM MitoTracker Green before analysis.

### ATP Measurement

ATP levels in GBM cells were measured using a luminescence ATP detection kit (Promega). Luminescence signals were detected using a microplate reader

(Synergy H1, BioTek Instruments). ATP levels were calculated from standard curves.

### LDH Production

The assay was quantified with a CytoTox 96 nonradioactive cytotoxicity assay kit (Promega) according to the manufacturer's instructions. The plates were incubated at room temperature for 30 min in the dark, and the absorbance was measured at 490 nm with a microplate reader (Synergy H1, BioTek). The LDH release values were normalized to cell number as determined by a cell counter (Life Technologies).

### Cell Metabolism Measurement

Cellular oxidative phosphorylation and glycolysis were monitored with the Seahorse Bioscience extracellular flux analyzer (XF24, Seahorse Bioscience) by measuring the OCR and ECAR in real time as described previously. Briefly, 15,000–25,000 cells were seeded in specific 24-well plates designed for XF24 in 250  $\mu$ L of the appropriate growth medium and incubated overnight. Prior to measurements, cells were washed with unbuffered medium once, immersed in 500  $\mu$ L of unbuffered medium, and incubated in the absence of CO<sub>2</sub> for 1 hr. The OCR and ECAR were then measured in a typical 8-min cycle of mix (2–4 min), dwell (2 min), and measure (2–4 min) as recommended by Seahorse Bioscience. The basal levels of OCR and ECAR were recorded first, and then the OCR and ECAR levels after sequential injection of compounds that inhibit the respiratory mitochondrial electron transport chain, ATP synthesis, or glycolysis were recorded.

### Relative mtDNA Content Measurements

The level of mtDNA was measured by assessing the relative levels of mtDNA-ND1 to nDNA-B3M using a PCR analysis of total DNA extracted from human GBM cells. The following amplification primers (Life Technologies) were used (5' to 3'): mtDNA-ND1 (sense, CCCTAAAACCGCCACATCT; antisense, GAGCGATGGTGAGAGCTAAGGT) and nDNA-B3M (sense, TGCTGTCTCC ATGTTTATGTATCT; antisense: TCTCTGCTCCCCACCTCTAAGT).

### Dual-Luciferase Reporter Assays

Luciferase reporter assays were conducted by cotransfecting U87MG cells with the firefly and *Renilla* luciferase plasmids. 48 hr post-transfection, cells were harvested, and the luciferase activity was measured using the Dual-Luciferase Reporter Assay System (Promega). Transcriptional activity was calculated as the ratio of firefly luciferase activity (reporter) to *Renilla* luciferase activity (control).

### PGC1 $\alpha$ Overexpression

The lentivirus was generated by co-transfection of the lentiviral expression plasmid expression PGC1 $\alpha$  (GeneCopoeia) or control vector together with the GeneCopoeia Lenti-Pac HIV expression packaging kit into HEK293T cells. The PGC1 $\alpha$ -overexpressing DBTRG-05MG cell line was established by stably transfecting DBTRG-05MG cells with the PGC1 $\alpha$ -overexpressing lentivirus and selecting with puromycin for 2 weeks.

## Figure 6. cAMP Activators Induce Tumor Growth Inhibition and Differentiation in GBM Xenograft Models and Patient-Derived GBM Samples

(A–C) Nu/nu mice were subcutaneously inoculated with U87MG (n = 7/group). 7 days after inoculation, mice were intraperitoneally treated with vehicle, forskolin (5 mg/kg/day), and luteolin (5 mg/kg/day). The tumor volume (means  $\pm$  SDs) was recorded every other day (A). 30 days after inoculation, the mice were killed and subjected to immunohistochemistry to evaluate the expression of Ki-67, PGC1 $\alpha$ , and GFAP (B and C).

(D and E) Nu/nu mice were intracranially inoculated with U87MG (n = 10/group). 3 days after inoculation, mice were intraperitoneally treated with vehicle and forskolin (5 mg/kg/day) or luteolin (5 mg/kg/day). 17 days after inoculation, we randomly selected two mice from every group to be killed for H&E staining of a brain cross-section (D). The survival times of the other mice in three groups were monitored until all of the mice were dead, and then a survival curve and Kaplan-Meier analysis were conducted (E).

(F–I) Primary patient-derived GBM cells were treated with dbcAMP for 48 hr, and then the GFAP expression level was measured by western blot (F) and immunofluorescence (G). dbcAMP also increased the mtDNA content (H) and the OCR (I) in primary GBM cells. Scale bar, 100  $\mu$ m. Data are presented as means  $\pm$  SDs (n = 3 per group).

(J and K) Nu/nu mice were intracranially inoculated with patient-derived GSCs (n = 10/group). 3 days after inoculation, mice were intraperitoneally treated with vehicle and forskolin (5 mg/kg/day). 17 days after inoculation, we randomly selected two mice from every group to kill for H&E staining of a brain cross-section (J). The survival times of the other mice in the three groups were monitored until all of the mice were dead, and then a survival curve and Kaplan-Meier analysis were conducted (K).

\*p < 0.05; \*\*p < 0.01; different from control group.

### Subcutaneous and Intracranial Xenograft GBM Models

Mice were housed in a pathogen-free animal facility. The hindflanks of 4-week-old female BALB/c-nu/nu mice were subcutaneously inoculated with  $2 \times 10^5$  U87MG cells. After 7 days, palpable tumors developed ( $50 \text{ mm}^3$ ), and the mice were randomly divided into three groups ( $n = 7$ ). These three groups were injected intraperitoneally once per day with vehicle, 5 mg/kg forskolin, or 5 mg/kg luteolin, respectively, for 14 days. Tumor diameters were measured every other day with a caliper, and tumor volumes were estimated using the following formula:  $\text{width}^2 \times \text{length}/2 = V \text{ (mm}^3\text{)}$ . Tumors were dissected and fixed in formalin for immunohistochemical analysis. Data are means  $\pm$  SD of 7 mice/group.

The orthotopic implantation of glioma cells was performed using  $3 \times 10^5$  U87MG cells or  $1 \times 10^5$  GSCs. In brief, cells were injected 2 mm lateral and 0.5 mm anterior to the bregma and 2.5 mm below the skull of 4-week-old athymic nude mice. After 3 days, the mice were randomly divided into two groups and injected intraperitoneally with vehicle or 5 mg/kg forskolin once per day for 14 days. The mice were monitored daily and killed when neurological symptoms were observed. Their brains were then dissected and fixed in formalin for H&E staining. A Kaplan-Meier survival curve was generated using the GraphPad Prism 6.0 software package (GraphPad). The points on the curves indicate glioma-related deaths ( $n = 8$  animals for each group;  $p$  was determined by log-rank analysis).

### Proteome Data Processing and Analysis

Protein identification and quantification were performed using MaxQuant v1.5.1.0 (Cox and Mann, 2008). The human protein sequence reference (GRCh38) was downloaded from Ensembl (Flicek et al., 2014), which contains 99,436 sequences. Carbamidomethylation was used for fixed modifications; methionine oxidation and N-terminal protein acetylation were used for variable modifications. Other settings used for peptide identification included a peptide false discovery rate of 0.01, minimum peptide length of seven amino acids, maximum miscleavages of 2. Only proteins annotated by at least two unique peptides were included for further analysis. Statistical analysis and plotting were done using in-house R codes.

### Transcriptome Data Processing and Analysis

Raw reads were trimmed to 90 nucleotides (nt) of length and were mapped to the UBSC human genome browser database (UCSC) hg19 reference genome (Lander et al., 2001) (<http://genome.ucsc.edu/>) using Tophat (v2.0.11) (Trapnell et al., 2009) (<http://tophat.cbcb.umd.edu/>). Default Tophat settings were used, except for the redefined parameter “-mate-inner-dist 200.” The inner distance between pair ends was estimated by the Picard program (<http://picard.sourceforge.net>). The HTSeq program was used to count mapped reads with the parameters “-s no -a 20” (Anders et al., 2015). Genes with less than two reads per million were removed, and 13,333 genes were included for further analysis. Gene count normalization and differential expression analysis were performed using the DESeq package (Anders and Huber, 2010).

### Gene Annotation and Functional Enrichment Analysis

The Piano package (Våremo et al., 2013) was used for GSEA (Subramanian et al., 2005). Gene sets were retrieved from Gene Ontology (<http://geneontology.org/>), Kyoto Encyclopedia of Genes and Genomes (KEGG), and the Ingenuity Pathways database (IPA, Ingenuity Systems, <http://www.ingenuity.com>) (Kanehisa and Goto, 2000; Kanehisa et al., 2014). Raw  $p$  values from the GSEA were corrected for multiple testing by false discovery rate (FDR). Pathways with corrected  $p$  values of less than 0.05 were considered significant.

### Statistical Analysis

Results in graphs are expressed as means  $\pm$  SD, as indicated in the figure legends, for the indicated number of observations. The data were analyzed with Student's  $t$  test (two-tailed, unequal variance). The tumor volume data were analyzed by a repeated-measure ANOVA. Animal survival time was analyzed by Kaplan-Meier process. Significance was defined as  $p < 0.05$ .

### ACCESSION NUMBERS

The accession number for the raw read data of RNA-seq reported in this paper is GEO: GSE89745. The accession number for the mass spectrometry proteomics data reported in this paper is ProteomeXchange Consortium: PXD005334 (Vizcaino et al., 2014).

### SUPPLEMENTAL INFORMATION

Supplemental Information includes six figures and can be found with this article online at <http://dx.doi.org/10.1016/j.celrep.2016.12.037>.

### AUTHOR CONTRIBUTIONS

F.X. and J.C. designed and performed the experiments and analyzed the data. Y. Luan performed the transcriptome and proteome data analysis. G.Y., W.Z., and Z.X. conceived the study and participated in the experimental design and in the analysis and interpretation of data. J.C., S.W., J.M., J.G., H.Z., K.L., Y. Lin, X.X., J.L., Y. Li, W.C., Y.T., L.S., B.L., W.L., M.G., P.Q., X.S., W.Y., J.H., Z.C., K.S., J.W., F.C., Y.C., S.Z., D.L., and S.C. contributed to data acquisition, interpretation, and data assembly. F.X., W.Z., and G.Y. edited the manuscript.

### ACKNOWLEDGMENTS

This work was supported by grants from the National Natural Science Foundation of China (81373428, 81673447, 81503088, and 31471232), the Natural Science Foundation of Guangdong Province (2014A030313156), the Fundamental Research Funds for the Central Universities (13ykpy07), the Joint Research Fund for Overseas Natural Science of China (3030901001222), the Major Program of Science and Technology of Guangzhou (201607020001), and the Science and Technology Planning Projects of Guangdong Province (2014B030301040). We would like to acknowledge Macmillan Science Communication (MSC) Scientific Editing and LetPub for editorial work.

Received: April 2, 2016

Revised: October 12, 2016

Accepted: December 9, 2016

Published: January 10, 2017

### REFERENCES

- Anders, S., and Huber, W. (2010). Differential expression analysis for sequence count data. *Genome Biol.* *11*, R106.
- Anders, S., Pyl, P.T., and Huber, W. (2015). HTSeq—a Python framework to work with high-throughput sequencing data. *Bioinformatics* *31*, 166–169.
- Bonnet, S., Archer, S.L., Allalunis-Turner, J., Haromy, A., Beaulieu, C., Thompson, R., Lee, C.T., Lopaschuk, G.D., Puttagunta, L., Bonnet, S., et al. (2007). A mitochondria-K<sup>+</sup> channel axis is suppressed in cancer and its normalization promotes apoptosis and inhibits cancer growth. *Cancer Cell* *11*, 37–51.
- Cairns, R.A., Harris, I.S., and Mak, T.W. (2011). Regulation of cancer cell metabolism. *Nat. Rev. Cancer* *11*, 85–95.
- Cassidy-Stone, A., Chipuk, J.E., Ingberman, E., Song, C., Yoo, C., Kuwana, T., Kurth, M.J., Shaw, J.T., Hinshaw, J.E., Green, D.R., and Nunnari, J. (2008). Chemical inhibition of the mitochondrial division dynamin reveals its role in Bax/Bak-dependent mitochondrial outer membrane permeabilization. *Dev. Cell* *14*, 193–204.
- Chang, B.D., Broude, E.V., Dokmanovic, M., Zhu, H., Ruth, A., Xuan, Y., Kandel, E.S., Lausch, E., Christov, K., and Roninson, I.B. (1999). A senescence-like phenotype distinguishes tumor cells that undergo terminal proliferation arrest after exposure to anticancer agents. *Cancer Res.* *59*, 3761–3767.
- Chau, M.D.L., Gao, J., Yang, Q., Wu, Z., and Gromada, J. (2010). Fibroblast growth factor 21 regulates energy metabolism by activating the AMPK-SIRT1-PGC-1 $\alpha$  pathway. *Proc. Natl. Acad. Sci. USA* *107*, 12553–12558.
- Cloughesy, T.F., Cavenee, W.K., and Mischel, P.S. (2014). Glioblastoma: from molecular pathology to targeted treatment. *Annu. Rev. Pathol.* *9*, 1–25.

- Cox, J., and Mann, M. (2008). MaxQuant enables high peptide identification rates, individualized p.p.b.-range mass accuracies and proteome-wide protein quantification. *Nat. Biotechnol.* **26**, 1367–1372.
- Dong, H., Siu, H., Luo, L., Fang, X., Jin, L., and Xiong, M. (2010). Investigation gene and microRNA expression in glioblastoma. *BMC Genomics* **11** (Suppl 3), S16.
- Flicek, P., Amode, M.R., Barrell, D., Beal, K., Billis, K., Brent, S., Carvalho-Silva, D., Clapham, P., Coates, G., Fitzgerald, S., et al. (2014). Ensembl 2014. *Nucleic Acids Res.* **42**, D749–D755.
- Folmes, C.D., Dzeja, P.P., Nelson, T.J., and Terzic, A. (2012). Metabolic plasticity in stem cell homeostasis and differentiation. *Cell Stem Cell* **11**, 596–606.
- Galluzzi, L., Kepp, O., Vander Heiden, M.G., and Kroemer, G. (2013). Metabolic targets for cancer therapy. *Nat. Rev. Drug Discov.* **12**, 829–846.
- Goldhoff, P., Warrington, N.M., Limbrick, D.D., Jr., Hope, A., Woerner, B.M., Jackson, E., Perry, A., Piwnica-Worms, D., and Rubin, J.B. (2008). Targeted inhibition of cyclic AMP phosphodiesterase-4 promotes brain tumor regression. *Clin. Cancer Res.* **14**, 7717–7725.
- Herzig, S., Long, F., Jhala, U.S., Hedrick, S., Quinn, R., Bauer, A., Rudolph, D., Schutz, G., Yoon, C., Puigserver, P., et al. (2001). CREB regulates hepatic gluconeogenesis through the coactivator PGC-1. *Nature* **413**, 179–183.
- Hock, M.B., and Kralli, A. (2009). Transcriptional control of mitochondrial biogenesis and function. *Annu. Rev. Physiol.* **71**, 177–203.
- Hsu, P.P., and Sabatini, D.M. (2008). Cancer cell metabolism: Warburg and beyond. *Cell* **134**, 703–707.
- Ito, K., and Suda, T. (2014). Metabolic requirements for the maintenance of self-renewing stem cells. *Nat. Rev. Mol. Cell Biol.* **15**, 243–256.
- Jahani-Asl, A., and Slack, R.S. (2007). The phosphorylation state of Drp1 determines cell fate. *EMBO Rep.* **8**, 912–913.
- Jiao, B., Ren, Z.-H., Liu, P., Chen, L.-J., Shi, J.-Y., Dong, Y., Ablain, J., Shi, L., Gao, L., Hu, J.-P., et al. (2013). 8-CPT-cAMP/all-trans retinoic acid targets t(11;17) acute promyelocytic leukemia through enhanced cell differentiation and PLZF/RAR $\alpha$  degradation. *Proc. Natl. Acad. Sci. USA* **110**, 3495–3500.
- Kanehisa, M., and Goto, S. (2000). KEGG: kyoto encyclopedia of genes and genomes. *Nucleic Acids Res.* **28**, 27–30.
- Kanehisa, M., Goto, S., Sato, Y., Kawashima, M., Furumichi, M., and Tanabe, M. (2014). Data, information, knowledge and principle: back to metabolism in KEGG. *Nucleic Acids Res.* **42**, D199–D205.
- Knott, A.B., Perkins, G., Schwarzenbacher, R., and Bossy-Wetzel, E. (2008). Mitochondrial fragmentation in neurodegeneration. *Nat. Rev. Neurosci.* **9**, 505–518.
- Koivunen, P., Lee, S., Duncan, C.G., Lopez, G., Lu, G., Ramkissoon, S., Losman, J.A., Joensuu, P., Bergmann, U., Gross, S., et al. (2012). Transformation by the (R)-enantiomer of 2-hydroxyglutarate linked to EGLN activation. *Nature* **483**, 484–488.
- Koppenol, W.H., Bounds, P.L., and Dang, C.V. (2011). Otto Warburg's contributions to current concepts of cancer metabolism. *Nat. Rev. Cancer* **11**, 325–337.
- LaGory, E.L., Wu, C., Taniguchi, C.M., Ding, C.-K.C., Chi, J.-T., von Eyben, R., Scott, D.A., Richardson, A.D., and Giaccia, A.J. (2015). Suppression of PGC-1 $\alpha$  Is Critical for Reprogramming Oxidative Metabolism in Renal Cell Carcinoma. *Cell Rep.* **12**, 116–127.
- Lander, E.S., Linton, L.M., Birren, B., Nusbaum, C., Zody, M.C., Baldwin, J., Devon, K., Dewar, K., Doyle, M., FitzHugh, W., et al.; International Human Genome Sequencing Consortium (2001). Initial sequencing and analysis of the human genome. *Nature* **409**, 860–921.
- LeBleu, V.S., O'Connell, J.T., Gonzalez Herrera, K.N., Wikman, H., Pantel, K., Haigis, M.C., de Carvalho, F.M., Damascena, A., Domingos Chinen, L.T., Rocha, R.M., et al. (2014). PGC-1 $\alpha$  mediates mitochondrial biogenesis and oxidative phosphorylation in cancer cells to promote metastasis. *Nat. Cell Biol.* **16**, 992–1003, 1–15.
- Leszczyniecka, M., Roberts, T., Dent, P., Grant, S., and Fisher, P.B. (2001). Differentiation therapy of human cancer: basic science and clinical applications. *Pharmacol. Ther.* **90**, 105–156.
- Li, Y., Yin, W., Wang, X., Zhu, W., Huang, Y., and Yan, G. (2007). Cholera toxin induces malignant glioma cell differentiation via the PKA/CREB pathway. *Proc. Natl. Acad. Sci. USA* **104**, 13438–13443.
- Losman, J.-A., Looper, R.E., Koivunen, P., Lee, S., Schneider, R.K., McMahon, C., Cowley, G.S., Root, D.E., Ebert, B.L., and Kaelin, W.G., Jr. (2013). (R)-2-hydroxyglutarate is sufficient to promote leukemogenesis and its effects are reversible. *Science* **339**, 1621–1625.
- Lu, C., Ward, P.S., Kapoor, G.S., Rohle, D., Turcan, S., Abdel-Wahab, O., Edwards, C.R., Khanin, R., Figueroa, M.E., Melnick, A., et al. (2012). IDH mutation impairs histone demethylation and results in a block to cell differentiation. *Nature* **483**, 474–478.
- Roninson, I.B. (2003). Tumor cell senescence in cancer treatment. *Cancer Res.* **63**, 2705–2715.
- Sancho, P., Burgos-Ramos, E., Tavera, A., Bou Kheir, T., Jagust, P., Schoenhals, M., Barneda, D., Sellers, K., Campos-Olivas, R., Graña, O., et al. (2015). MYC/PGC-1 $\alpha$  Balance Determines the Metabolic Phenotype and Plasticity of Pancreatic Cancer Stem Cells. *Cell Metab.* **22**, 590–605.
- Stork, P.J., and Schmitt, J.M. (2002). Crosstalk between cAMP and MAP kinase signaling in the regulation of cell proliferation. *Trends Cell Biol.* **12**, 258–266.
- Stupp, R., Mason, W.P., van den Bent, M.J., Weller, M., Fisher, B., Taphoorn, M.J., Belanger, K., Brandes, A.A., Marosi, C., Bogdahn, U., et al.; European Organisation for Research and Treatment of Cancer Brain Tumor and Radiotherapy Groups; National Cancer Institute of Canada Clinical Trials Group (2005). Radiotherapy plus concomitant and adjuvant temozolomide for glioblastoma. *N. Engl. J. Med.* **352**, 987–996.
- Subramanian, A., Tamayo, P., Mootha, V.K., Mukherjee, S., Ebert, B.L., Gillette, M.A., Paulovich, A., Pomeroy, S.L., Golub, T.R., Lander, E.S., and Mesirov, J.P. (2005). Gene set enrichment analysis: a knowledge-based approach for interpreting genome-wide expression profiles. *Proc. Natl. Acad. Sci. USA* **102**, 15545–15550.
- Trapnell, C., Pachter, L., and Salzberg, S.L. (2009). TopHat: discovering splice junctions with RNA-Seq. *Bioinformatics* **25**, 1105–1111.
- Väremo, L., Nielsen, J., and Nookaew, I. (2013). Enriching the gene set analysis of genome-wide data by incorporating directionality of gene expression and combining statistical hypotheses and methods. *Nucleic Acids Res.* **41**, 4378–4391.
- Vazquez, F., Lim, J.H., Chim, H., Bhalla, K., Girnun, G., Pierce, K., Clish, C.B., Granter, S.R., Widlund, H.R., Spiegelman, B.M., and Puigserver, P. (2013). PGC1 $\alpha$  expression defines a subset of human melanoma tumors with increased mitochondrial capacity and resistance to oxidative stress. *Cancer Cell* **23**, 287–301.
- Vizcaíno, J.A., Deutsch, E.W., Wang, R., Csordas, A., Reisinger, F., Ríos, D., Dianes, J.A., Sun, Z., Farrah, T., Bandeira, N., et al. (2014). ProteomeXchange provides globally coordinated proteomics data submission and dissemination. *Nat. Biotechnol.* **32**, 223–226.
- Ward, P.S., and Thompson, C.B. (2012). Metabolic reprogramming: a cancer hallmark even warburg did not anticipate. *Cancer Cell* **21**, 297–308.
- Warrington, N.M., Gianino, S.M., Jackson, E., Goldhoff, P., Garbow, J.R., Piwnica-Worms, D., Gutmann, D.H., and Rubin, J.B. (2010). Cyclic AMP suppression is sufficient to induce gliomagenesis in a mouse model of neurofibromatosis-1. *Cancer Res.* **70**, 5717–5727.
- Warrington, N.M., Sun, T., Luo, J., McKinstry, R.C., Parkin, P.C., Ganzhorn, S., Spoljaric, D., Albers, A.C., Merkelson, A., Stewart, D.R., et al. (2015). The cyclic AMP pathway is a sex-specific modifier of glioma risk in type I neurofibromatosis patients. *Cancer Res.* **75**, 16–21.
- Weller, M., Pfister, S.M., Wick, W., Hegi, M.E., Reifenberger, G., and Stupp, R. (2013). Molecular neuro-oncology in clinical practice: a new horizon. *Lancet Oncol.* **14**, e370–e379.
- Yang, L., Jackson, E., Woerner, B.M., Perry, A., Piwnica-Worms, D., and Rubin, J.B. (2007). Blocking CXCR4-mediated cyclic AMP suppression inhibits brain tumor growth in vivo. *Cancer Res.* **67**, 651–658.